IEEE Access
Multidisciplinary | Rapid Review | Open Access Journal

Received June 26, 2020, accepted July 7, 2020, date of publication July 20, 2020, date of current version August 10, 2020.

Digital Object Identifier 10.1109/ACCESS.2020.3010551

Outage of Millimeter Wave Links With Randomly Located Obstructions

AMR A. ABDELNABI[1,2], VINCENZO MANCUSO[2], (Member, IEEE), AND MARCO AJMONE MARSAN[2,3], (Life Fellow, IEEE)

[1]Telematic Engineering Department, Universidad Carlos III de Madrid (UC3M), 28911 Getafe, Spain
[2]IMDEA Networks Institute, 28918 Leganés, Spain
[3]Electronics and Telecommunications Department, Politecnico di Torino, 10129 Torino, Italy

Corresponding author: Amr A. AbdelNabi (amr.abdelnabi@imdea.org)

This work was supported in part by the Region of Madrid through the Técnicas Avanzadas para Potenciar la Inteligencia de las Redes 5G - Comunidad de Madrid (TAPIR-CM) Program under Grant S2018/TCS-4496. The work of Vincenzo Mancuso was supported by the Ramon y Cajal from the Spanish Ministry of Economy and Competitiveness under Grant RYC-2014-16285.

ABSTRACT According to current regulation, millimeter wave links can only rely on low transmission power, which calls for high gain steerable antenna arrays to generate very directional beams bringing signals of detectable power to the intended receiver. However, beam directionality, jointly with the very limited scattering and diffracting capabilities of millimeter waves, implies high sensitivity to obstructions, which can cause link outage. This article proposes new analytical models for the estimation of the outage probability of millimeter wave indoor and outdoor links, based on the derivation of the distribution of the obstruction length along the beam. To derive the models, we use stochastic geometry and assume randomly located obstructions. The proposed models are used to explore the impact on millimeter wave link performance of a number of parameters such as distance between transmitter and receiver, obstruction shape and size, density of obstructions, carrier frequency and modulated bandwidth. The models can be used to study realistic 2D and 3D scenarios, and are shown to be quite accurate by comparing analytical predictions and simulation results in numerous cases.

INDEX TERMS Millimeter wave communications, modeling, performance evaluation, random obstructions, outage probability, stochastic geometry.

I. INTRODUCTION

According to the latest Cisco Annual Internet Report [2], ''there will be 13.1 billion mobile connected devices by 2023'', and ''the average mobile connection speed will grow 3.3-fold from 2018 to 2023, from 13.2 Mbps in 2018 to 43.9 Mbps by 2023''. Besides, Ericsson analysts forecast that the total mobile traffic (uplink plus downlink) will experience a continuous growth of over 27% a year until 2025 [3], not yet accounting for the traffic boost due to the current COVID-19 pandemic. The net result is an increase in traffic which is much faster than the increase in mobile connection speed. This traffic growth is congesting the frequency bands below 6 GHz, which are used today for mobile communications, and is making the spectrum available for data communications insufficient. Thus, exploiting higher frequency bands (tens of GHz to THz) will soon become necessary to satisfy the hunger for wireless data transfer. In addition, applications considered for 5G radio access networks and beyond, e.g., augmented/virtual reality and the tactile wireless internet, require data transfers at rates of a few Gbps per individual end user, with quite challenging requirements on latency and reliability [4].

In this context, the need to support the mobile traffic growth and carry multi-Gbps base-band signals, makes the millimeter wave (mmwave) technology [5] a necessity for upcoming radio access networks, starting with 5G [6].

The propagation characteristics of mmwave channels are radically different from sub-6 GHz channels. Sub-6 GHz signals are able to travel longer distances and better penetrate solid objects with respect to mmwave signals. In fact, the Friis transmission equation shows that path-loss increases quadratically with wavelength, and also reflections from a surface depend on the wavelength of the signal. This implies that in

The associate editor coordinating the review of this manuscript and approving it for publication was Ding Xu.

the case of mmwave, reflections carry signals much weaker than what delivered over the line-of-sight (LoS) path [7].[1] Indeed, experimental studies have shown that the received mmwave signal is mainly composed by the LoS component plus what received from first-order reflection paths only [8], which can be described with a quasi-deterministic propagation model [9].

Since narrow beams are characteristic of mmwave systems, and mmwaves are highly sensitive to attenuation caused by materials of common use, from wood to glass and plastics, as well as water and organic matter, it is imperative to carefully model the impact of obstructions on the mmwave link outage. More specifically, as pointed out in [6], mmwave outage occurs because of four main reasons: first, penetration losses are very severe with commonly used materials; second, mmwaves tend to bend around obstructions instead of being diffracted; third, the narrow beams used to ensure the necessary directionality weaken the ability to avoid obstructions; fourth, the low transmission power used for mmwaves does not leave much signal to noise ratio (SNR) margin to avoid outage.

Nonetheless, when a path is obstructed, a detectable and decodable signal might still reach the receiver after traversing small portions of one or more obstructions, or by the aid of attenuated reflections or even limited diffraction and scattering effects [6]. These effects are typically neglected in available performance studies and models, although they may effectively help achieving high reliability of the mmwave system. We therefore focus on modeling and evaluating two key aspects: the attenuation due to one or more obstructions over the LoS path, and the influence of available (although possibly obstructed) reflection paths for narrow-beam mmwave transmissions. This study is essential for the design of mmwave networks since it sheds light on the importance of accounting for multiple obstructions and for beamforming algorithms that could exploit reflections.

A. RELATED WORK

Incorporating models of outage into the analytical framework for mmwave system design is important, since outage significantly impacts design choices. Outage is usually modeled by considering self-body outage effects [10] and shadowing effects, whose impact can be represented by means of a lognormal random variable (r.v.). In [11], the authors use ray tracing to model mmwave outage in a deterministic environment. In [12], a random Boolean line segment process is used to model heights of random outdoor obstructions. The authors assume that blockage is Boolean, i.e., it occurs when any obstruction lies on the path between transmitter and receiver. This model has been further specified for rectangular [13] and circular obstruction shapes [14]. Our models improve with respect to these approaches since they are neither deterministic nor Boolean, allowing to stochastically quantify the attenuation due to sets of obstructions.

The above mentioned studies and many of the available ones deal with outdoor environments. As regards indoor environments, most papers are based on measurements, and report up to 80 dB loss at 73 GHz for half-meter-long obstructions and 40 dB for a 28-cm depth human body [15], [16]. In [17], the authors present obstruction measurements, fitting them with various statistical models. However, their resulting model is based on a specific measurement scenario, hence it may not be able to explain the results observed in other scenarios. In this paper we provide instead a more general approach to outage estimation.

Based on what is known about attenuation, some authors have developed more complex outage models. The authors of [18] use queuing theory to model the duration of (self) blockage in the presence of macro-diversity in the transmission schemes. The authors of [19] discuss the influence of randomly distributed wall blockages on the downlink of an indoor cellular network. They consider randomly distributed obstructions, each causing a fixed amount of attenuation. In [20], the authors derive a stochastic model of human blockage by means of a ray-launching simulator that is capable of dealing with time-variant scenarios. They address an indoor scenario with realistic person movements, and suggest that LoS and blockage duration can be described by Weibull distributions. In [21], the authors aim to minimize blockage in the network and minimize the maximum load across all base stations in the network. A new concept called blockage score is defined, using a record of the points in the coverage area where blockage occurred in the past. Such record is used to predict future outages (where an event is counted as outage if the signal power goes below a defined threshold). This methodology of blockage detection lacks an explicit description of the obstacle itself, and of its impact on outage. More in general, differently from our work, existing proposals neither model the effects of per-obstacle attenuation on overall outage occurrence, nor consider the geometric properties of obstructions.

The work in [22] explores the impact of randomly located obstruction by considering that the obstruction either totally blocks the signal or reflects it. However, in practice, the signal can also penetrate and cross the obstruction, depending on the material of the obstruction and the obstruction length, which is what we instead include in our models.

More specifically, motivated by previous research in this area, we present the first work that accounts for the possibility that outage is caused by the accumulated attenuation due to more than one obstruction over any of the paths that beamsteering can select in the presence of quasi-deterministic propagation. Our early results were presented in [1], where we have shown how to estimate the outage probability based on a simple 2D model of the average length of the portion of a path that is occupied by obstructions. In there, we account for LoS paths as well as reflections with a very simplified model

[1] We use the term path to indicate the possible route of the mmwave beam carrying data from transmitter to receiver; a path can be direct (LoS) or include reflections. The term link refers instead to the data connection from transmitter to receiver, that uses one of the possible paths, the one with lowest attenuation.

of the individual obstruction contribution to path attenuation (i.e., by considering that each obstruction causes the same attenuation, computed based on the average chord length of the obstruction shape). Here we significantly extend and generalize that model to a more precise description of individual obstruction contributions to path loss, also considering more realistic 3D cases.

B. OUR CONTRIBUTION

With respect to the existing body of work, this paper includes the following novel pieces of contribution.

- We derive simple yet accurate and tractable expressions to characterize the cumulative obstruction length caused by multiple objects between a transmitter and a receiver on both LoS and reflected paths, as well as the corresponding attenuation. This provides a significant improvement with respect to existing models that either consider the presence of an obstruction as a binary decision variable that causes outage, or consider the actual attenuation due to an obstruction but do not account for the compound effect of multiple obstructions at all.
- We derive stochastic geometry-based models for the mmwave link outage probability that account for the effect of reflections and beamsteering, considering the possibility to select the best path among LoS and reflections. The use of stochastic geometry allows estimating the performance of mmwave links in the presence of randomly located obstructions. Although we only consider paths with just primary reflections, our modeling approach can accommodate successive reflections as well.
- We present accurate and tractable expressions for the outage probability caused by any kind of obstruction in 2D and 3D spaces, unlike other works that focused only on 2D obstructions. We show that the 3D case yields better performance than 2D in many cases in terms of spectral efficiency and average data rate, mainly because of the presence of a higher number of reflected paths.
- We provide examples of the application of our approach to a wide portion of the mmwave spectrum, from 18 to 73 GHz, providing useful insight on the design of mmwave systems in environments with randomly located obstructions.

C. PAPER ORGANIZATION

The paper is organized as follows. The system model is described in Section II. In Section III, we characterize the obstruction caused by randomly located objects. In Section IV, we derive new outage probability models, based on two different approximations for the obstruction caused by each object. Numerical results are presented in Section V. Finally, we summarize our results and findings in Section VI.

D. BASIC NOTATION

We denote by $\Pr(A)$ the probability of event A. $F_X(\cdot)$ is the cumulative distribution function (CDF) of r.v. X. $f_X(\cdot)$ is the corresponding probability density function (pdf). $\mathcal{M}_X(\cdot)$ is the moment generating function (MGF) of the r.v. X. The term $u(\cdot)$ denotes the unit step function, while $\delta(.)$ represents the Dirac delta function. The notation used in the paper is summarized in Table 1.

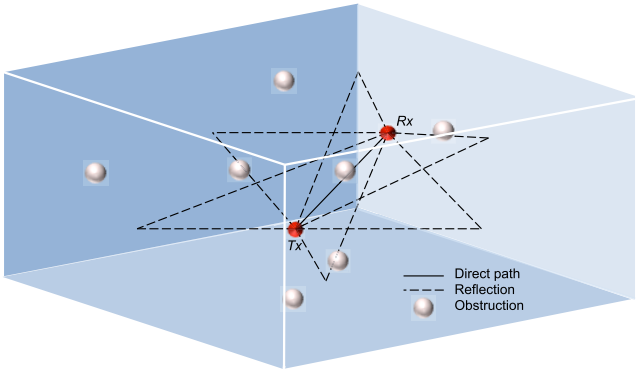

FIGURE 1. Layout for direct path and reflections for a 3D case with spherical obstructions.

II. SYSTEM MODEL

We consider a wireless communication system consisting of a mmwave transmitter/receiver pair, i.e., one access point (Tx node) and one user equipment (Rx node), placed at fixed known locations, within a 2D or 3D rectangular (parallelepipedal in 3D) walled environment. The mmwave signal can be reflected by walls (including roof and ceiling, in the 3D case), so that in addition to the direct (LoS) path between Tx and Rx, reflection paths exist, as illustrated in FIGURE 1 in a 3D case.

We consider a quasi-deterministic channel model [9] with a direct path and a limited number (normally 4 for 2D and 6 for 3D) of primary reflections, i.e., paths with a single reflection, caused by a wall.

A random number of objects are randomly placed in the walled environment and may obstruct mmwave paths.

Transmitter and receiver are assumed to be aligned thanks to beamsteering, and antennas are considered strongly directional, so that antenna side lobes are negligible. The beamsteering alignment is assumed to be the optimal one in terms of SNR (signal to noise ratio), which does not necessarily correspond to the LoS path between Tx and Rx, which indeed might be obstructed. In any case, beamsteering perfectly aligns Tx and Rx according to either the LoS or any of the available primary reflection paths. Since beamsteering is fast and can be tuned frequently, at millisecond time scale as done by currently available IEEE 802.11ad mmwave devices [23], we assume that beamsteering always selects the least attenuated path.

In our performance analysis, the lengths of the considered paths are the components of a vector $\vec{d}$, in which the first element is the LoS distance between Tx and Rx, and the remaining elements list the lengths of primary reflection paths in a fixed order.

TABLE 1. Notation used in this article.

Notation	Description
d_k	Length of path k.
$\vec{d}$	Vector containing the lengths of the considered paths, i.e., $d_1 \dots d_k$.
k	Path index ($k = 1$ for LoS).
d	LoS path length ($k = 1$), thus $d = d_1$ for simplicity.
P_t	Transmit power.
G	Antenna gain after beamsteering including both Tx and Rx antenna gains.
L_k	Path loss for path k in dB.
c	Speed of light in the air in m/s.
f	Adopted mmwave frequency in GHz.
A_O	Air absorption loss due to the transmission medium in dB/m.
W_k	Wall attenuation on the selected path k in dB.
h	Unit power small scale fading (for path k, $1/\mu_k$ is a constant that represents the actual fading power).
X_k	Total obstruction length travelled by the signal on path k.
$a(X_k)$	Total average attenuation on path k, in dB units.
σ^2	Noise variance.
γ_k	SNR after steering the antennas to align with path k.
Ψ	R.v. representing the minimum of the path losses observed over LoS and a set of primary reflections.
γ	SNR after beamsteering to the best selected path.
N_k	Average number of obstructions for path k.
l_o	Average obstruction length.
z	Obstruction loss per unit length in dB/m.
B	Inverse power-to-noise ratio before attenuation ($\frac{\sigma^2}{P_\mathrm{t}G}$) .
R_k	Measure of the sensitive region, where R_1 is for LoS.
U, A_2	Perimeter of 2D obstruction and surface of 2D obstruction.
A_3, V	Surface and volume of a 3D obstruction.

A. SNR COMPUTATION

The path loss L_k on path k is modeled considering free-space loss, air absorption and reflection loss. In dB units, the loss is:

$$L_k = 20\log_{10}(4\pi f d_k/c) + A_\mathrm{O} d_k + W_k, \tag{1}$$

where A_O depends on frequency and medium composition (we consider standard air, in which absorption is mainly due to the presence of oxygen), and W_k is the wall attenuation on the selected path in dB ($W_1 = 0$ dB, since the direct path does not suffer reflections), which depends on frequency, materials and reflection angles.

We assume an idealized case of perfect matching between the transmitter antenna impedance and the channel impedance; if this is not the case, rather than considering the power transmitted by the antenna we must consider the power actually injected into the medium.

Reflections of mmwave signals on walls suffer attenuation according to their polarization, frequency, refraction indices of air and wall, and angle of incidence of the reflected wave on the wall. Specifically, the attenuation W_k is computed by means of the well-known Fresnel equations, which yield different values for each of the walls, depending on the materials considered for the walls and the specific geometry of the studied case.

The effect of an obstruction on the mmwave signal can be of different types: reflection, refraction or blocking, or a mix of them. Here, we focus on the blocking effect, assuming negligible reflection and refraction, as customary for mmwave systems. We model in particular the additional attenuation produced by obstructions along the signal path. Considering the mmwave propagation characteristics through dielectric [24], the length of the intersection between a path and an obstruction (that we call *per-object obstruction length*) yields a signal attenuation of z dB/m, where the value of z depends on the obstruction material and the frequency. The r.v. X_k models the *total obstruction length* over path k, i.e., the sum of per-object obstruction lengths due to individual objects that intersect the path.

The channel coefficient for a path is denoted by h/μ_k, in which the r.v. h captures the normalized path small scale fading, and is modeled as a Rayleigh distributed [2] r.v., so that $|h|^2$ is an exponential r.v. with mean 1. The factor $1/\mu_k$ is a constant that represents the average fading depth [9] The total average attenuation on path k, not considering the small scale fluctuations due to h, is a r.v. $a(X_k)$ that depends on X_k. Thus, in dB units, the average attenuation is the sum of all attenuation components [24], which are path loss, average fading depth and attenuation due to obstructions:

$$a(X_k) = L_k + 10\log_{10}\mu_k + zX_k. \tag{2}$$

Noise is assumed to be additive Gaussian with variance σ^2, so that, by putting together all the pieces, the SNR γ_k, after steering the antennas to align with path k, is:

$$\gamma_k = \frac{P_\mathrm{t} G\,|h|^2}{\sigma^2} 10^{\frac{-a(X_k)}{10}}. \tag{3}$$

[2] While our model assumes Rayleigh fading on all paths, in simulations we use Rice distributions for the LoS path fading.

If antennas are optimally steered at each transmission, the experienced SNR will therefore correspond to the SNR of the path that suffers the least average attenuation. This means that, once the positions of Tx, Rx and walls are known, and obstructions are placed, the beamsteering is deterministic and fixed, depending only on the path loss and the obstruction attenuation, plus an average loss due to small scale fading. Therefore, the SNR after beamsteering can be expressed as a function of the small scale fading h and of a r.v. Ψ that accounts for the fact that beamsteering selects the path that minimizes path loss $a(X_k)$:

$$\Psi = \min_k \left\{ 10^{a(X_k)/10} \right\}. \tag{4}$$

The resulting expression for the SNR is as follows:

$$\gamma = \frac{P_t G |h|^2}{\sigma^2 \Psi}. \tag{5}$$

B. RANDOMLY LOCATED OBSTRUCTIONS

We assume that the positions of obstructions "centers" within the considered 2D or 3D area follows a 2D or 3D Poisson Point Process (PPP) with given intensity λ. We define the "center" of an obstruction as the mid point on its maximal transverse dimension. The process that describes the positions of obstructions of any of the paths is therefore a PPP as well, obtained by restricting the original PPP. We consider that such PPPs are independent of each other. This is reasonable for the case in which the probability that an object obstructs more than one path is negligible. Under this assumption, the joint distribution of the number of obstructions over the available paths is simply the product of the distributions for each of the individual paths. Hence, for a vector $\vec{n}$ of elements $\{n_k\}$, containing the number of objects obstructing the direct path and the primary reflection paths, the joint probability distribution is a joint Poisson distribution, i.e.:

$$\Pr(\vec{n}) = e^{-\sum_k N_k} \cdot \prod_k \frac{(N_k)^{n_k}}{n_k!}, \tag{6}$$

where N_k is the average number of obstructions on path k.

III. CHARACTERIZATION OF OBSTRUCTION IMPACT

The propagation characteristics of mmwave signals and the use of directional beamforming, plus the fact that scattering and diffraction can be neglected for mmwaves, while they are important for microwaves and lower frequency bands, make the models presented in this article applicable to mmwaves but unsuitable for lower frequencies. Note also that the strong attenuation suffered by mmwave signals after successive reflections make it possible to characterize the interference in a quasi-deterministic way (i.e., there is interference only if a beam hits a receiver in the LoS direction), which is not the case for sub-mmwave bands. Likewise, there are strong differences between mmwaves and visible light in terms of propagation, especially for what concerns scattering and reflections, so we cannot re-use visible light models for characterizing propagation and blockage in mmwave systems. Our models can however be partially applied to sub-millimeter communications—THz frequencies above the mmwave spectrum and below the infrared frequencies—although using THz bands is strongly affected by the absorption due to H_2O [25], which would require some modifications in our equations. Moreover, THz transmission techniques, and beamforming for THz antennas in particular, are still in their infancy, so we prefer to let them out of the scope of our work.

In the reminder of this section we use stochastic geometry to derive some key parameters for evaluating mmwave blockage, hence computing the outage probability. We start by identifying and characterizing the region in which objects can cause obstruction, so as to derive a simple stochastic model for the number of obstructions over a path between transmitter and receiver. The average of this r.v., which is denoted as N_k for path k, affects the link selection probability, as seen in Section II-B. Therefore we derive expressions for the average N_k. In addition, we derive an expression for the average total obstruction length, which will be used in the computation of the mmwave link outage in the next section.

Note that since mmwaves suffer high attenuation, only scenarios with low density of obstructions are interesting. Hence, in our analysis we assume that randomly placed obstructions do not overlap, which is reasonable for the case in which the size of obstructions is small with respect to the path length.

A. SENSITIVE REGION

The possibility that an object becomes an obstruction depends on the distance between its center and the segment(s) describing the path. In particular, if the maximal transverse dimension of the object is t, only objects with center within $t/2$ from the path can cause obstruction. We use this consideration to restrict the PPP of the obstruction centers to a specific path. Accordingly, we define as "sensitive region" of a path the portion of the 2D or 3D space in which randomly placed centers of objects with random rotation can cause obstruction. We denote by R_1 the average measure of the sensitive region for the LoS path and $R_k, k > 1$ the average measure corresponding to reflected paths. The measures of regions are averaged over all possible rotations of the obstructions. This is useful because the average number of obstructions, with obstructions distributed according to a homogeneous PPP, is proportional to the average measure of the sensitive region.

In 2D, the sensitive region of a LoS path of length d is comprised in a rectangle with sides t and $d + t$. Similarly, in 3D, we have a cylinder with base of diameter t, and height $d + t$. However, we further consider that obstructions cannot overlap with Tx and Rx. As a consequence, given an object shape and a fixed rotation, there exist two regions around Tx and Rx in which no obstruction center can lay.

As it is easy to see, the average measure of the resulting region is $\bar{y} \cdot d$ minus the measure of the obstruction itself (i.e., either its area or volume), where $\bar{y}$ is the average projection

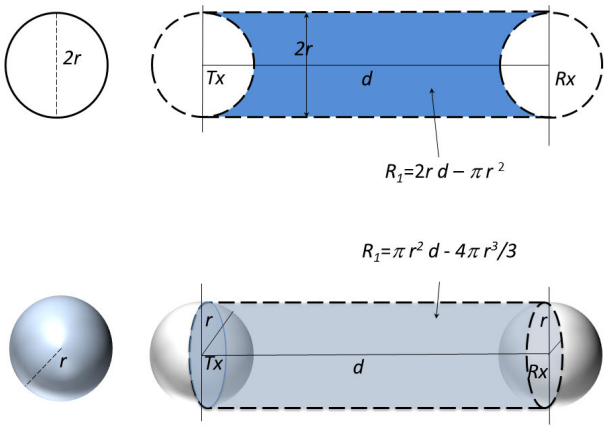

FIGURE 2. Sensitive region for circular and spherical obstructions: obstruction centers can only lay within the shaded regions.

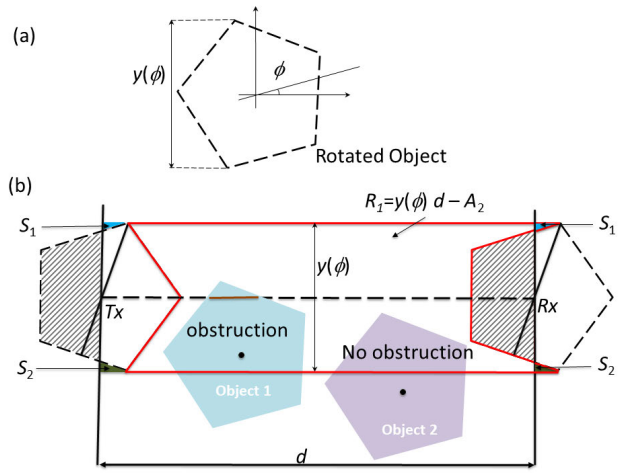

FIGURE 3. (a) Rotated pentagon, (b) Sensitive region for pentagons: obstruction centers can only lay within the red contour line.

of the obstruction shape with respect to the sub-space orthogonal to the direction of the path. As an example, the topmost part of FIGURE 2 shows R_1 for circular obstructions in the 2D case, while the bottom part of the figure shows the sensitive region in the 3D case, for spherical obstructions. FIGURE 3 depicts the case of a pentagonal object, for a fixed rotation angle ϕ. In particular, FIGURE 3 (b) shows the sensitive region for a LoS path, for objects with the shape (and rotation) of FIGURE 3 (a). In the figure, the sensitive region is delimited by a red line. The center of Object 1 lies inside the red boundaries, hence it causes obstruction by intercepting the LoS link. Instead, Object 2 is not an obstruction because, although it overlaps the sensitive region, its center lies outside the red boundaries, and therefore the pentagon does not intercept the LoS link. Note that the shape of the sensitive region is not regular. However, due to the symmetries of the example, the small triangles indicated at the top corners have both area S_1, and the two at the bottom have area S_2, so that the measure of the sensitive region is the same as the one of the rectangle built on the LoS link, with a height equal to $y(\phi)$, which is the projection of the pentagon over the direction orthogonal to the LoS link. Such rectangular area would however include two complementary sections of the area of a pentagon, one to the left of the transmitter and one to the right of the receiver, where no center of obstruction can be present (otherwise the obstruction would occupy the space of the transmitter or the receiver). This justifies the term $-A_2$ in the 2D formula of (8) for the area of the sensitive region shown in the figure.

The examples commented above are valid each for a fixed shape and a fixed rotation of the object that can cause obstruction. In general, the measure of the sensitive region will be different for each object and rotation. However, since we are interested in the average number of obstructions that can be present, and such number is proportional to the measure of the sensitive region, it will be enough to consider the average measure of the sensitive region over the possible object shapes and rotations. Note that the only quantities that change with the object are its measure, and, depending on the rotation, its projection over the space orthogonal to the considered link. So, for a given shape, we need to characterize such projection.

When rotations matters (i.e., except for circles in 2D and spheres in 3D), we therefore need to compute the average projection of the obstruction shape over the continuous set of possible rotations in either the 2D or 3D space. To this aim we can use the Cauchy's surface area formula (that has been generalized to any number of dimensions [26]):

$$\bar{y} = \begin{cases} \dfrac{U}{\pi} & \text{for 2D;} \\ \dfrac{A_3}{4} & \text{for 3D;} \end{cases} \tag{7}$$

This result is valid for the orthogonal projection of any 2D line of length U with respect to a random direction, and for the projection of any 3D surface of measure A_3 with respect to a random projection plane. Hence, the formula holds also for closed curves and surfaces representing the perimeter or the closed surface of an object rotated uniformly at random.

As a consequence, the measure of R_1 can be always expressed as follows:

$$R_1 = \begin{cases} d\cdot\bar{y} - A_2 = d\cdot\dfrac{U}{\pi} - A_2 & \text{for 2D;} \\ d\cdot\bar{y} - V = d\cdot\dfrac{A_3}{4} - V & \text{for 3D;} \end{cases} \tag{8}$$

In our analysis we will use the same computation for all paths, using the total length of the path after reflection, R_k, and neglecting border effects that slightly reduce the measure of the sensitive region, hence the number of randomly located obstructions counted next to the reflection point.

B. EXPRESSIONS FOR CONVEX OBJECTS

For the special case of objects with convex shape, the average conditional per-object obstruction length l_o can be computed by means of the second Cauchy formula [11], which expresses the relation between the average chord length and

the geometrical properties of an object:

$$l_o = \begin{cases} \frac{\pi A_2}{U} & \text{for 2D;} \\ \frac{4V}{A_3} & \text{for 3D;} \end{cases} \quad (9)$$

As a consequence, the sensitive region can be expressed as a function of l_o, as follows:

$$R_k = \begin{cases} (d_k/l_o - 1)\, A_2 & \text{for 2D;} \\ (d_k/l_o - 1)\, V & \text{for 3D.} \end{cases} \quad (10)$$

C. AVERAGE NUMBER OF PER-PATH OBSTRUCTIONS

The number of obstructions intersecting the LoS path (but the same is true for all paths) has Poisson distribution. This is clear for a fixed object shape and rotation, because the number of objects that fall in a deterministic space region, with a uniform PPP, is Poisson. Thus, by assuming that the object shape is fixed and the rotation is uniformly picked at random, the r.v. that models the number of obstructions is the weighted sum of independent Poisson r.v.'s, and it is therefore a Poisson r.v. itself. As a result, the number of obstructions on path k has a Poisson distribution with average denoted by N_k which can be written as

$$N_k = \lambda R_k, \quad (11)$$

where λ is the rate of the Poisson process that defines the positions of obstructions centers.

D. AVERAGE TOTAL OBSTRUCTION LENGTH

The average for the total obstruction length on a path is taken to be the sum of a random, Poisson distributed, number of independent per-object obstruction lengths. We remark that this is appropriate for obstruction densities such that the average obstruction length is much less than the path length. The average total obstruction length on path k, denoted by O_k, can be thus expressed as follows:

$$O_k = e^{-N_k} \sum_{n_k=0}^{\infty} \frac{N_k^{n_k}}{n_k!} n_k l_o = N_k l_o = \lambda R_k l_o, \quad (12)$$

which, for convex obstructions, becomes

$$O_k = \begin{cases} \lambda\, (d_k - l_o)\, S_2 & \text{for 2D;} \\ \lambda\, (d_k - l_o)\, V & \text{for 3D.} \end{cases} \quad (13)$$

IV. OUTAGE PROBABILITY

The outage probability P_{out} is defined as the probability that the SNR γ takes a value below a given threshold γ_{th} in a scenario defined by physical transmission parameters plus obstruction effects. Next, we derive a generic expression for the outage probability, then we propose two approximate expressions, one based on the average per-object obstruction length and one in which the distribution of the per-object obstruction length is approximated with a weighted Dirac comb. Both cases work for generic obstruction shapes.

A. GENERAL EXPRESSION

The outage probability can be derived from (5) and corresponds to the CDF of the r.v. $|h|^2/\Psi$ evaluated in $B\gamma_{\text{th}}$, where $B \stackrel{\text{def}}{=} \frac{\sigma^2}{P_t G}$ is a constant:

$$P_{\text{out}}(\gamma_{\text{th}}) = \Pr\left(\frac{P_t G}{\sigma^2}\frac{|h|^2}{\Psi} \le \gamma_{\text{th}}\right) = \Pr\left(\frac{|h|^2}{\Psi} \le B\gamma_{\text{th}}\right)$$
$$\stackrel{(a)}{=} \int_0^{\infty} \left(1 - e^{-B\gamma_{\text{th}} x}\right) f_\Psi(x) dx = 1 - \mathcal{M}_\Psi(-B\gamma_{\text{th}}), \quad (14)$$

where (a) comes from the fact that $|h|^2$ is exponentially distributed (since h has Rayleigh distribution) and we have applied the total probability formula to the distribution of Ψ. Therefore, if the pdf or the MGF of Ψ are known, the above formulas can be used to obtain the link outage probability.

However, the distribution and the MGF of Ψ are in general difficult to obtain, since Ψ is the minimum path attenuation, so that its CDF is a function of the set of CDFs $\{F_k(x)\}$, i.e., of the CDFs of the fading-averaged attenuation on each path,[3] and each corresponding pdf $f_k(x)$ is the weighted convolution of a random number of fading-averaged attenuation pdf's, one for each individual and independent obstruction. This calls for approximations of the pdf of individual obstruction lengths with the objective of simplifying the computation of the convolutions. The attenuations on different paths can be considered independent, since we assumed that the numbers of obstructions on the available paths are independent r.v.'s. Therefore, the complementary CDF of Ψ, which is the minimum path attenuation, is the product of the complementary CDF's of the path attenuation r.v.'s, i.e.:

$$1 - F_\Psi(x) = \prod_k (1 - F_k(x)). \quad (15)$$

The pdf $f_\Psi(x)$ can be obtained as the derivative of $F_\Psi(x)$, so to finally evaluate the outage through (14). In general, this procedure requires a numerical approach to the evaluation of distribution functions as well as to compute derivatives and integrals. However, we next propose two approximations which lead to the derivation of closed form expressions for the distribution of Ψ, and which permit solving the integral in (14) in closed form as well.

B. AVERAGE-BASED APPROXIMATION

A very simple approximation can be obtained by representing each object with its average obstruction length. With this approximation, the total attenuation resulting from n obstructions on the k-th path, assuming the antennas are steered on that path, is simply expressed as

$$a(X_k|n) = L_k + 10\, \log_{10} \mu_k + z\, n\, l_o, \quad (16)$$

under the assumption of having obstructions covering small fractions of the lengths traveled by the mmwaves, and for

[3]We remark that Ψ only depends on the average fading, while the effect of fading variations is modeled through h.

negligible probability for one object to obstruct more than one path. The probability to use path i is therefore

$$\pi_i = \sum_{\vec{n}=\vec{0}}^{\infty} \Pr(\vec{n}) \Pr(i = \arg\min_k \{a(X_k|n)\}) = e^{-\sum_k N_k} \sum_{n_i=0}^{\infty} \frac{N_i^{n_i}}{n_i!} \prod_{k\neq i} \sum_{n_k=n_k^{(i)}}^{\infty} \frac{N_k^{n_k}}{n_k!}, \quad (17)$$

where $\Pr(\vec{n})$ is the joint Poisson distribution in (6) and the minimum index value in the rightmost sum is the smallest integer number of objects on path k such that the attenuation on path i is smaller than on path k, i.e.:

$$n_k^{(i)} = \max\left\{0, \left\lceil n_i + \frac{L_i - L_k}{z a_k} + \frac{10}{z a_k} \log_{10} \frac{\mu_i}{\mu_k} \right\rceil\right\}. \quad (18)$$

Thus, the number of obstructions completely describes the per-path total obstruction length. Being the number of obstructions Poisson, the resulting path attenuation r.v. is described by masses of probability of amplitude equal to the weights of a Poisson distribution, centered at $\mu_k 10^{\frac{L_k + z n_k l_o}{10}}$, $n_k \geq 0$ (in linear units). Therefore, the pdf of the path attenuation can be written as follows:

$$f_k(x) = e^{-N_k} \sum_{n_k=0}^{\infty} \frac{N_k^{n_k}}{n_k!} \delta\left(x - \mu_k 10^{\frac{L_k + z n_k l_o}{10}}\right). \quad (19)$$

The complementary CDF of Ψ, which is the minimum path attenuation, is the product of the complementary CDF's of the path attenuation r.v.'s, i.e.:

$$1 - F_\Psi(x) = \prod_k \left(1 - e^{-N_k} \sum_{n_k=0}^{\infty} \frac{N_k^{n_k}}{n_k!} u\left(x - \mu_k 10^{\frac{L_k + z n_k l_o}{10}}\right)\right).$$

The pdf of Ψ, namely $f_\Psi(\cdot)$, is obtained by calculating the derivative of $F_\Psi(\cdot)$ as follows:

$$\begin{aligned} f_\Psi(x) &= \sum_i \sum_{n_i=0}^{\infty} e^{-N_i} \frac{N_i^{n_i}}{n_i!} \delta\left(x - \mu_i 10^{\frac{L_i + z n_i l_o}{10}}\right) \cdot \prod_{k\neq i} \left(1 - e^{-N_k} \sum_{n_k=0}^{\infty} \frac{N_k^{n_k}}{n_k!} u\left(x - \mu_k 10^{\frac{L_k + z n_k l_o}{10}}\right)\right) \\ &= \sum_i \sum_{n_i=0}^{\infty} e^{-N_i} \frac{N_i^{n_i}}{n_i!} \delta\left(x - \mu_i 10^{\frac{L_i + z n_i l_o}{10}}\right) \cdot \prod_{k\neq i} \left(1 - e^{-N_k} \sum_{n_k=0}^{\infty} \frac{N_k^{n_k}}{n_k!} u\left(\mu_i 10^{\frac{L_i + z n_i l_o}{10}} - \mu_k 10^{\frac{L_k + z n_k l_o}{10}}\right)\right) \\ &= e^{-\sum_k N_k} \sum_i \sum_{n_i=0}^{\infty} \frac{N_i^{n_i}}{n_i!} \delta\left(x - \mu_i 10^{\frac{L_i + z n_i l_o}{10}}\right) \prod_{k\neq i} \sum_{n_k=n_k^{(i)}}^{\infty} \frac{N_k^{n_k}}{n_k!}. \end{aligned} \quad (20)$$

By plugging this result into (14), we obtain an approximate formula for the outage probability:

$$P_{\text{out}}(\gamma_{\text{th}}) = 1 - e^{-\sum_k N_k} \sum_i \sum_{n_i=0}^{\infty} \frac{N_i^{n_i}}{n_i!} e^{-B\gamma_{\text{th}}\mu_i 10^{\frac{L_i + z n_i l_o}{10}}} \prod_{k\neq i} \sum_{n_k=n_k^{(i)}}^{\infty} \frac{N_k^{n_k}}{n_k!}. \quad (21)$$

C. WEIGHTED DIRAC COMB-BASED APPROXIMATION

A more accurate approximation for the per-object obstruction length distribution is based on the use of a weighted Dirac comb for the chord length pdf:

$$f_\ell(x) \simeq \sum_{i=1}^{M} \alpha_i \delta(x - a_i), \quad (22)$$

with masses of probability located at $a_i \in [0, s], \forall i \in \{1, \ldots, M\}$, where s is the length of the maximum transverse dimension of the obstruction. The term α_i indicates the probability mass located at a_i. To work with less parameters, it is convenient to space the Dirac delta functions so that all masses are the same, i.e., $\alpha_i = 1/M$. So, we split the support of the actual chord distribution $f_\ell(x)$ into M intervals, such that each interval accumulates exactly a probability $1/M$ and we approximate the pdf in each interval with a single Dirac delta located at the point that corresponds to the conditional average of the distribution within that interval. With the above, the approximated pdf yields the same average as the original one. Note also that, if we use $M = 1$, we obtain the average-based approximation described in the previous subsection. Therefore, what we are describing in this subsection is a generalization of what described before. While the average per-object obstruction length (at least for convex objects) can be always computed with the Cauchy formula, the exact expression for the pdf $p(x)$ is only known for some regular shapes (see the Appendix for some 2D and 3D cases). In the general case, $p(x)$ can be experimentally or numerically derived, so to allow for the computation of the coefficients. The pdf of the total obstruction length due to n objects is obtained by taking the n-fold convolution of $f_\ell(x)$. If $q(x|n)$ denotes such pdf, we have:

$$q(x|n) = p^{*n}(x) \simeq \frac{1}{M^n} \sum_{i_1=1}^{M} \cdots \sum_{i_n=1}^{M} \delta\left(x - \sum_{j=1}^{n} a_{i_j}\right). \quad (23)$$

The corresponding attenuation is obtained considering that the attenuation is a bijective function of the obstruction length, according to (2). Therefore, the pdf for the attenuation observed in the presence of n objects on path k is obtained by using a weighted Dirac comb like in (23), except now the mass probabilities are moved from a_i to $\mu_k 10^{\frac{L_k + z a_i}{10}}$, i.e., $\forall n \geq 1$:

$$f_k(x|n) = \frac{1}{M^n} \sum_{i_1=1}^{M} \cdots \sum_{i_n=1}^{M} \delta\left(x - \mu_k 10^{\frac{L_k + z \sum_{w=1}^{n} a_{i_w}}{10}}\right). \quad (24)$$

Moreover, in case of no obstructions, the attenuation is deterministic for each path: [4]

$$f_k(x|n=0) = \delta\left(x - \mu_k 10^{\frac{L_k}{10}}\right). \tag{25}$$

The pdf of the total path attenuation is obtained by averaging the above expression over the value of n, as follows:

$$f_k(x) = e^{-N_k}\left[\delta\left(x-\mu_k 10^{\frac{L_k}{10}}\right) + \sum_{n=1}^{\infty}\frac{(N_k/M)^n}{n!}\sum_{i_1=1}^{M}\cdots\sum_{i_n=1}^{M}\delta\left(x-\mu_k 10^{\frac{L_k+z\sum_{w=1}^{n}a_{i_w}}{10}}\right)\right]. \tag{26}$$

The corresponding CDF is as follows:

$$F_k(x) = e^{-N_k}\left[u\left(x-\mu_k 10^{\frac{L_k}{10}}\right) + \sum_{n=1}^{\infty}\frac{(N_k/M)^n}{n!} \times \sum_{i_1=1}^{M}\cdots\sum_{i_n=1}^{M}u\left(x-\mu_k 10^{\frac{L_k+z\sum_{w=1}^{n}a_{i_w}}{10}}\right)\right]. \tag{27}$$

Since ψ is the minimum of the r.v.'s with distribution $f_k(\cdot)$, the following result holds:

$$f_\psi(x) = \sum_k\left[f_k(x)\prod_{j\neq k}\left(1-F_j(x)\right)\right]. \tag{28}$$

Replacing (26) and (27) into (28), after some simple manipulation of the expressions, we obtain the following pdf:

$$\begin{aligned} f_\psi(x) = {} & \sum_k e^{-N_k}\delta\left(x-\mu_k 10^{\frac{L_k}{10}}\right) \\ & \cdot\prod_{j\neq k}\left(1-e^{-N_j}\left(u\left(\mu_k 10^{\frac{L_k}{10}}-\mu_j 10^{\frac{L_j}{10}}\right)\right.\right. \\ & +\sum_{n_j=1}^{\infty}\frac{(N_j/M)^{n_j}}{n_j!} \\ & \left.\left.\sum_{t_1=1}^{M}\cdots\sum_{t_{n_j}=1}^{M}u\left(\mu_k 10^{\frac{L_k}{10}}-\mu_j g_1\right)\right)\right) \\ & +\sum_k e^{-N_k}\sum_{n_k=1}^{\infty}\frac{(N_k/M)^{n_k}}{n_k!}\sum_{i_1=1}^{M}\cdots\sum_{i_{n_k}=1}^{M}\delta\left(x-\mu_k g_2\right) \\ & \cdot\prod_{j\neq k}\left(1-e^{-N_j}\left(u\left(\mu_k g_2-\mu_j 10^{\frac{L_j}{10}}\right)\right.\right. \\ & +\sum_{n_j=1}^{\infty}\frac{(N_j/M)^{n_j}}{n_j!} \\ & \left.\left.\sum_{t_1=1}^{M}\cdots\sum_{t_{n_j}=1}^{M}u\left(\mu_k g_2-\mu_j g_1\right)\right)\right), \end{aligned} \tag{29}$$

[4]Here we are interested in characterizing Ψ, i.e., which path offers the least average attenuation, so to be selected by beamforming; hence fading is considered in terms of its average $1/\mu_k$, and the only remaining source of randomness is due to the presence and positions of obstructions.

where we have used the following definitions:

$$\begin{cases} g_1(L_j, n_j, a_{t_w}) & = 10^{\frac{L_j+z\sum_{w=1}^{n_j}a_{t_w}}{10}}; \\ g_2(L_k, n_k, a_{i_w}) & = 10^{\frac{L_k+z\sum_{w=1}^{n_k}a_{i_w}}{10}}. \end{cases}$$

Let $O(n_i, \vec{i})$ denote the total obstruction length due to n_i obstructions each of which contributing a_{i_ℓ} to the obstruction length, with $\vec{i} = \{i_\ell\}_{\ell=1}^{n_i}$, with $\vec{i}$ representing a generic permutation of n_i indices that range from 1 to M, and $O(0, \vec{i}) = 0$ with no indices to permute (i.e., one single possible configuration). With the above notation, the outage probability derived by plugging (29) into (14) can be expressed as follows:

$$\begin{aligned} & P_{\text{out}}(\gamma_{\text{th}}) \\ & = 1-\sum_k e^{-N_k}\sum_{n_k=0}^{\infty}\frac{(N_k/M)^{n_k}}{n_k!}\sum_{\vec{v}}e^{-B\gamma_{\text{th}}\mu_k 10^{\frac{L_k+z\,O(n_k,\vec{v})}{10}}} \\ & \cdot\prod_{j\neq k}\left(1-e^{-N_j}\sum_{n_j=0}^{\infty}\frac{(N_j/M)^{n_j}}{n_j!}\right. \\ & \left.\cdot\sum_{\vec{w}}u\left(\mu_k 10^{\frac{L_k+z\,O(n_k,\vec{v})}{10}}-\mu_j 10^{\frac{L_j+z\,O(n_j,\vec{w})}{10}}\right)\right). \end{aligned} \tag{30}$$

D. INSIGHTS ON AVERAGE-BASED APPROXIMATION AND WEIGHTED DIRAC COMB-BASED APPROXIMATION

In what follows, the simple model based on the average-based approximation is referred to as AVG, while we use WDC to indicate the model that builds on top of the weighted Dirac comb-based approximation. The first model is simpler but rougher. Indeed, AVG can be obtained from WDC when we consider a single Dirac delta in the comb used to approximate the distribution of per-object obstruction length. In general, the only difference between the two models comes from the use of either one or more terms in the Dirac delta comb. However, using just one term (in AVG) has allowed us to reach a more compact closed-form result than for the generic case (the one of WDC).

1) COMPLEXITY

The higher M, i.e., the number of Dirac deltas used in WDC, the higher the accuracy of the approximation, and the higher the complexity of the model, because the number of sums to be computed for each value of k and n_k goes with M^{n_k}, as it can be observed by inspecting, e.g., the expression for the distribution of Ψ in (29). AVG yields the lowest complexity, but it still requires to compute an infinite number of coefficients, which are Poisson coefficients combined with products of truncated exponential functions. Indeed, both AVG and WDC account for any number of obstructions, with a Poisson distribution. However, the probability of having a high number of obstructions is practically negligible, and so the summations on n_k can be truncated as soon as the term $\frac{(N_k/M)^{n_k}}{n_k!}$ becomes negligible. In practice, with the characteristics of mmwave attenuation, even with small objects obstructing a few cen-

timeters, it is sufficient to consider a few objects, no more than 5 with the scenarios considered in the numerical evaluation session presented in this paper. Interestingly, the higher M, the lower the number of obstructions that practically need to be accounted for in the numerical evaluation of the WDC model, which only partially counterbalances the power-law growth in the number of sums required for each value of the number of obstructions.

Although the model complexity is not negligible, this is not a critical aspect of our approach. in fact, our models are meant to run offline, and no real-time decisions depend on them. However, we remark that the models can be numerically solved with inexpensive hardware in limited time. For instance, a set of model curves like the ones reported in FIGURE 6, which comprises 4 curves each for AVG and WDC, and 121 points per curve, were obtained in 21 seconds using AVG and in 72 seconds using WDC on a Dell Latitude E7470 equipped with Intel Core i7, 2.6 GHz CPU and 8 GB RAM, running a single threaded instance of Matlab R2019b.

2) INTERPRETATION OF THE MODELS

The outage formulas of AVG and WDC reveal that the complement to 1 of the outage probability can be approximated by using weighted exponential functions of the outage threshold, with progressively decreasing amplitude due to the attenuation of the considered combination of obstructions. The number of Dirac deltas used in the approximations determines the number of exponential functions to be used. Hence, we can expect that increasing M yields smoother curves, while using AVG we can expect to observe some staircase shape in the outage curves, with each step due to the cut-off of a different exponential function. Moreover, since each exponential function of γ_{th} in both (21) and (30) expresses the contribution to outage due to a particular geometrical combination, the formulas tell that the curves of outage probability vs γ_{th} evolve in smoothed steps, according to the probability that the signal strength exceeds the attenuation due to the total obstruction length of a given geometrical configuration, from the configuration with the highest attenuation (i.e., the exponential with the smaller cut-off threshold, which is the least likely) to the one with the lowest incurred attenuation (which is not necessarily the least likely geometrical configuration). A good trade-off between accuracy and complexity, to estimate the shape of the outage curve, consists in identifying geometrical configurations that incur non-negligible attenuation and occur with non-negligible probability. This is exactly what AVG does when truncating the sum over n_k to a few obstructions.

These behavior trends will be clearly visible in the numerical results presented in the next section. For instance, FIGURE 4 and FIGURE 5 clearly show that increasing the number of Dirac deltas increases the accuracy of the model for both 2D and 3D, and that using AVG can result in excessive step-like artifacts in the curve of the modeled outage probability. Still, the accuracy of AVG is sufficient for analyzing at least the order of magnitude for the probability that an outage will occur.

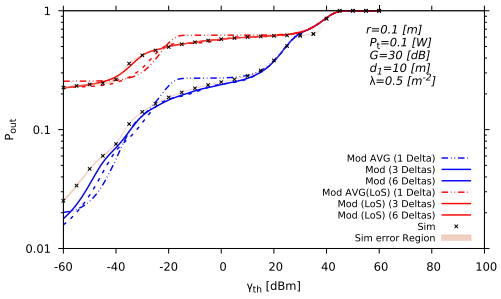

FIGURE 4. Model and simulation with 95% confidence intervals estimates of outage probability in a 20m × 30m 2D space, for circular obstructions, computed for direct path and for the case of selecting always the least attenuated path, vs the SNR threshold γ_{th} for different number of dirac deltas.

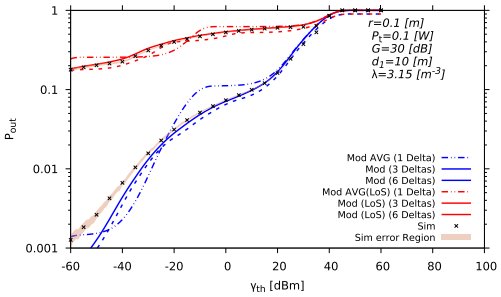

FIGURE 5. Model and simulation with 95% confidence intervals estimates of outage probability in a 20m × 30m × 3m space, for spherical obstructions, computed for direct path and for the case of selecting always the least attenuated path, vs the SNR threshold γ_{th} for different number of dirac deltas.

V. NUMERICAL RESULTS

In this section, we compare the accuracy of the approximations proposed in the previous section, and we use our model to explore the performance of mmwave links in some representative cases: (*i*) we consider the 2D indoor case, with possible reflections on four walls; (*ii*) we explore the 3D indoor case, with possible reflections on six planes; (*iii*) we consider the 2D outdoor street case, with reflections on the buildings at the sides of a street. We also evaluate the spectral efficiency and the average rate achievable at different mmwave frequencies.

We numerically evaluate our models and compare their predictions to the results of a Monte Carlo simulator written in Matlab, which accounts for randomly placed obstructions, without approximations. The simulator considers unit Rayleigh fading for reflection paths, and Rice fading for LoS, with scale parameter equal to 1 and shape parameter equal to 10 (i.e., unit fading with LoS power component 10 times higher than reflection components), as recommended for mmwave links with beamforming [27]. Average simulation results are presented together with their 95% confidence intervals [28]. Here we use the model to evaluate a mmwave link under the assumption that Tx and Rx are fixed and

TABLE 2. Typical values of obstruction attenuation z and air absorption loss A_O at various frequency values [29].

Frequency (f)	Obstruction attenuation (z)	Air absorption (A_O)
18 GHz	130 dB/m	0.00006 dB/m
26 GHz	200 dB/m	0.00013 dB/m
60 GHz	390 dB/m	0.015 dB/m
73 GHz	420 dB/m	0.0075 dB/m

obstructions are homogeneous in shape and type (same geometry, same material). However, the model can be also used for evaluating snapshots of systems with moving Tx and Rx, and can use any statistical description of obstruction shapes (i.e., by using the chord length distribution corresponding to a given mix of shapes, and the average measure of the sensitive region). The examples we report here represent a set of meaningful scenarios that allow the evaluation of the accuracy of the model and shed light on the properties of the system. However, the list of examples is not, and cannot be, by any means exhaustive.

We consider two possibilities for the mmwave link beamsteering. In the first case, the direct (LoS) path is always selected (this corresponds to using only $k = 1$ in our model), while in the second case the path where the attenuation is the lowest is selected (this can be the direct path or one of the reflected paths, and the selection does not account for fading fluctuations, only the average fading is considered).

A. THE 2D INDOOR CASE

For all the results that we present in this case, except when otherwise specified, we consider a room of width 20 m and length 30 m, which is represented as a rectangle over a plane with origin at the lower left corner of the rectangle; using 1 m units, the mmwave transmitter is placed at coordinates (1, 1), and the receiver is placed at distance d, at $(1 + d/\sqrt{2}, d/\sqrt{2} + 1)$. Except for plots as a function of d, we will use $d = 10$ m. Except for plots as a function of λ, the intensity of the PPP governing the presence of obstructions is set to $\lambda = 0.5$ m^{-2}, which corresponds to slightly less than one obstruction, on average, over a 10 m long LoS path. We report results for circular and square obstructions. Except for plots as a function of r, circles have radius $r = 0.1$ m, so that they can represent common objects or even portions of human bodies. Squares have the same area as circular obstructions. We assume realistic values for the unit fading power (i.e., $\mu = 1$), total antenna gain ($G = 30$ dB),[5] transmission power ($P_t = 0.1$ W), noise floor level ($\sigma^2 = 1.65 \cdot 10^{-11}$ W), and refractive indices equal to 1 for air and 1.5 for walls (which is close to the one of many materials used for construction). The values for air absorption A_O, obstruction attenuation z and

[5] G is obtained by considering a gain of 20 dB at the transmitter and 10 dB at the receiver, as suggested in [6].

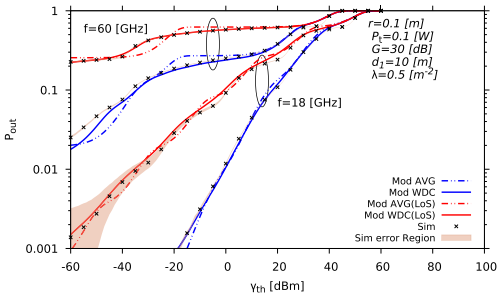

FIGURE 6. Model and simulation with 95% confidence intervals estimates of outage probability in a 2D room of 20m × 30m, for circular obstructions, for two mmwave frequencies, computed for direct path and for the case of selecting always the least attenuated path, versus the SNR threshold γ_{th}.

operating frequency f are selected based on experimentally determined values, as listed in Table 2.

FIGURE 6 and FIGURE 7 show for circular and square obstructions, respectively, the curves of the estimates of P_{out} generated with (21) for the simple approximation case (AVG) and with (30) for the weighted Delta comb case (WDC). The figures also show Matlab simulation results. Both model and simulation show that the outage can be quite high for SNR values in a range from 0 to 20 dB, which roughly corresponds to thresholds commonly required to enable higher bit per second per Hz modulation and coding schemes in today's real devices. However, outage is clearly not an on/off function of the presence of obstructions, since different SNR thresholds yield smoothly different outage probabilities. The outage experienced at the higher frequency is the highest, which is consistent with the fact that the coefficient z at 60 GHz is three times higher than at 18 GHz, while the air absorption coefficient plays a very minor role.

A comparison between the two figures reveals that considering circular rather that square objects does not significantly change performance figures. Moreover, the gain offered by beamsteering over reflected paths is huge, as it is equivalent to improve SNR by tens of dBs. Indeed, selecting the least attenuated path with beamsteering largely outperforms a simplistic approach based on blindly using the direct path (indicated as AVG(LoS) and WDC(LoS) in the figures). This happens notwithstanding the fact that reflected paths are longer and incur much higher path loss levels, which can however be less impairing than the presence of obstructions on the direct path, unless reflected paths are obstructed as well. Therefore, in the following figures, we will only focus on the performance of the system in the presence of a beamsteering that can select any of the LoS and reflected paths.

The figures also clearly show that the model with the weighted Dirac comb (WDC) outperforms the one that uses the average obstuction length only (AVG). In fact, despite the good accuracy of the simple approximation based on the average obstruction length, especially for lower outage values, the figures show that WDC is much more accurate in general as it produces smoother curves, while the simple approximation used in AVG yields a kind of staircase-shaped

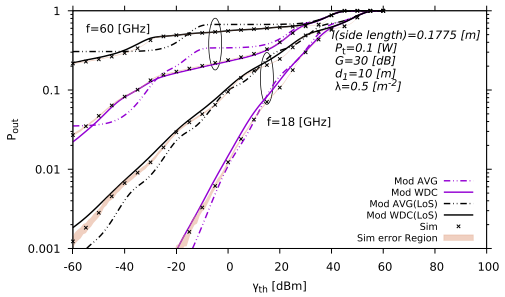

FIGURE 7. Model and simulation with 95% confidence intervals estimates of outage probability in a 2D room of 20m ×30m, for square obstructions, for two mmwave frequencies, computed for direct path and for the case of selecting always the least attenuated path, versus the SNR threshold γ_{th}.

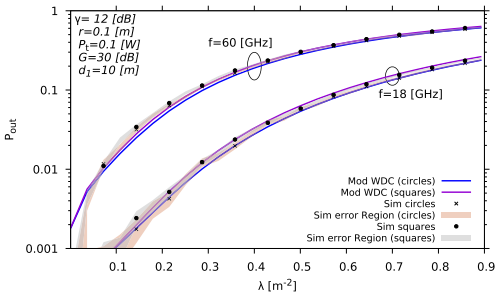

FIGURE 8. Model and simulation with 95% confidence intervals estimates of outage probability in a room of 20m ×30m, for circular and square obstructions, for two values of frequency, versus λ, for best path selection.

curves. Since the difference between AVG and WDC is substantial, and a comparison with simulations shows that WDC is more accurate, in the following, we will only consider WDC.

The better accuracy of WDC is obtained at the expense of a higher computation complexity, which is the natural consequence of the more complicated structure of (30) with respect to (21). Specifically, the complexity of each term of (21), i.e., for each value of i and n_i is basically the complexity of computing one exponential function and a limited number of products, [6] while computing one term of (30), i.e., for fixed k and n_k, has the complexity of computing an exponential for M^{n_k} permutation cases, and for each permutation, one has to add at least the complexity of the entire (21) repeated as many times as the number of considered paths minus one. In practice, summations in both formulas can be stopped at small values, as soon as the exponential terms fade. In this numerical evaluation, the maximum average number of obstructions that we consider per link, in both (21) and (30), is 5, which is the average number of obstructions over the longest reflected path studied in this article. Although limiting the numerical analysis to this number leaves out obstruction configurations which can occur with non-negligible probability, the high values of z make it very unlikely that a path obstructed by 5 or more objects can be of use. We have numerically tested that using up to 4 objects instead of 5, all curves reported in this study would move by at most 0.3%, while using 6, the maximum amplitude change we observed in the curves was below 0.1%. Such relative variations are in addition observed for very small values of the outage probability. Therefore we used 5 objects for all cases, since the effect of considering a larger number of obstructions on the numerical results that we present in this section is marginal. [7]

Another parameter that can be tuned to trade off accuracy for complexity is M, i.e., the number of Dirac delta functions used to approximate the per-object obstruction length. In the derivation of the results presented in this section we used $M = 6$ since we have observed that the marginal improvement in accuracy obtained by increasing M is a decreasing function, and using 6 Dirac deltas instead of 5 for the results in FIGURE 7, we obtained a marginal improvement as low as 1.7% over tiny probability values, so that further increasing M yielded differences that could not be practically appreciated.

FIGURE 8 reports model and simulation results as we vary obstruction density λ, while FIGURE 9 illustrates how the outage depends on the obstruction size (by varying the circle radius r, hence the side of the square with equivalent area). In these figures, we fix the value of the SNR threshold γ_{th} so to provide a reasonable data throughput performance. With currently available devices, the 16 QAM modulation scheme provides reasonable data rate performance and requires about 12 dB of SNR [30], therefore we use $\gamma_{\text{th}} = 12$ dB.

In FIGURE 8, we see the effect of increasing λ, which obviously implies an increase of the outage probability for both frequencies considered in the figure. The model accurately follows simulation results, and there is no major difference between the case with circles and the one with squares. For both considered frequencies, the outage probability goes to zero with λ, although with a very different slope, due to large differences in the obstruction attenuation z. Also in this case, the outage at higher frequencies is consistently much higher than at lower ones.

FIGURE 9 shows that, as expected, the increase in obstruction size degrades performance as it increases the chance of having longer obstruction length. Also, the increase of obstruction size with the increase of attenuation loss z increases the outage probability. This applies to both circular and square obstructions, which show similar performance, regardless of the frequency used.

FIGURE 10 shows the effect of distance between transmitter and receiver on outage probability. Here we have fixed again the SNR threshold to 12 dB. The increase of the direct path length results in a net increase of reflected path lengths, which in turn results in having higher attenuation with higher number of obstructions on all of the paths that can be used for the Tx-Rx link. The figure shows that frequencies

[6] Note that the infinite sum in the rightmost part of (21), $\sum_{n_k=n_k^{(i)}}^{\infty} \frac{N_k^{n_k}}{n_k!}$, can be computed with a finite number of terms as $e^{N_k} - \sum_{n_k=0}^{n_k^{(i)}-1} \frac{N_k^{n_k}}{n_k!}$

[7] Note that most of the previous models only considered the presence (or absence) of one single obstruction.

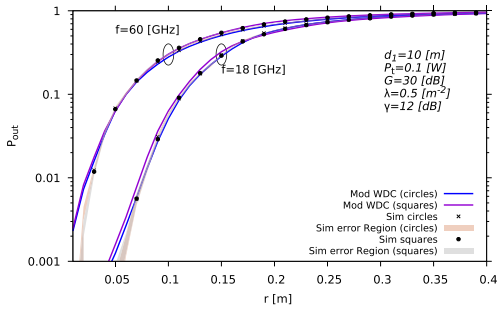

FIGURE 9. Model and simulation with 95% confidence intervals estimates of outage probability in a room of 20m ×30m, for circular and square obstructions, for two values of frequency, versus obstruction size, for the best path selection.

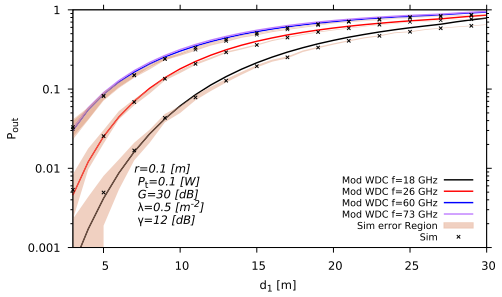

FIGURE 10. Model and simulation with 95% confidence intervals estimates of outage probability in a room of 20m ×30m, for circular obstructions, for different frequencies and their corresponding values of z, versus d_1, for best path selection.

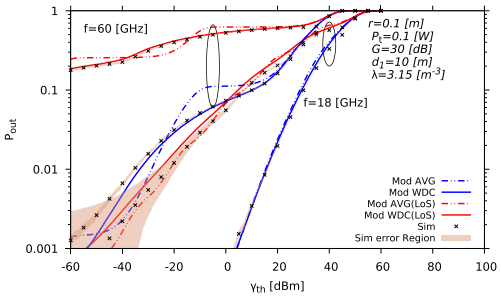

FIGURE 11. Model and simulation with 95% confidence intervals estimates of outage probability in a 3D room of 20m ×30m × 3 m, for spherical obstructions, for two mmwave frequencies, computed for direct path and for the case of selecting always the least attenuated path, versus the SNR threshold γ_{th}.

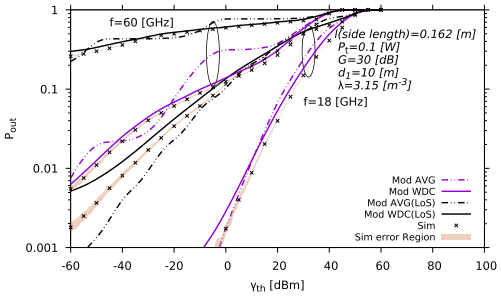

FIGURE 12. Model and simulation with 95% confidence intervals estimates of outage probability in a 3D room of 20m ×30m ×3m, for cubic obstructions, for two mmwave frequencies, computed for direct path and for the case of selecting always the least attenuated path, versus the SNR threshold γ_{th}.

in the high end side of the considered range behave quite similarly. Instead, the outage observed at lower frequency is much lower at all distances. With the realistic parameters we have used, stochastically obstructed mmwave links can be reliably used only for short distances: for instance, with a target outage of at most 0.1, $\lambda = 0.5$ and $r = 0.1$ m, higher frequencies cannot be used with more than about 6 m between transmitter and receiver, while at 18 GHz it is possible to communicate as far as 12.5 m.

B. THE 3D INDOOR CASE

We now consider a 3D room of width 20 m, length 30 m and height 3 m, which is represented as a rectangular parallelepiped. This is the same scenario as in the previous case, except we now consider a third spatial dimension. Transmission, reflection and attenuation parameters, as well as transmission power, refractive indices and noise are like in the 2D case. Using 1 m units, the mmwave transmitter is placed at coordinates (1, 1, 1), and the receiver is placed at distance d, at coordinates $(1 + d/\sqrt{2}, 1 + d/\sqrt{2}, 1)$. Except for plots as a function of d, we will use $d = 10$ m. Except for plots as a function of λ, the intensity of the PPP governing the presence of obstructions is set to $\lambda = 3.15$ m^{-3} which provides the same average number of obstructions per path length as in the 2D indoor case. We report results for spherical and cubic obstructions. Spheres have radius 0.1 m, while cubes have the same volume as spherical obstructions.

FIGURE 11 and FIGURE 12 show the curves of the estimates of P_{out} generated by (21) for AVG and by (30) for WDC as well as by simulation for spherical and cubic obstructions, respectively. These figures report results for the 3D extension of what shown in FIGURE 6 and FIGURE 7 for the 2D case.

Also in this case, WDC clearly outperforms AVG in terms of accuracy. Indeed, the improvement offered by WDC is much more remarkable in the 3D case, where AVG is not always able to provide decent outage estimates, especially for the case of cubic obstructions. Although the qualitative behavior of the outage probability vs. SNR threshold is similar in the two cases, the outage in 3D is much lower than in 2D, for a given SNR threshold. The reason of such difference is twofold: (*i*) the 3D case offers more reflection alternatives (6, with respect to 4 in the 2D case), and (*ii*) the average obstruction length due to a 3D extension of a regular 2D shape is smaller than the one of the 2D object. This happens because, in the 3D case, what counts is the 2D shape that is obtained by intersecting the 3D object with the planes on which transmitter, receiver and reflection points lay. The result is that, in 3D, the profile of the obstruction seen over a projection plane is with high probability smaller than with the regular 2D shape used as reference (for circles/spheres, the probability is exactly 1). For example, simple math shows that the ratio $l_o(\text{circle})/l_o(\text{sphere}) = \frac{3\pi}{8}$, which means that the per-object obstruction length due to a circle is 15% more

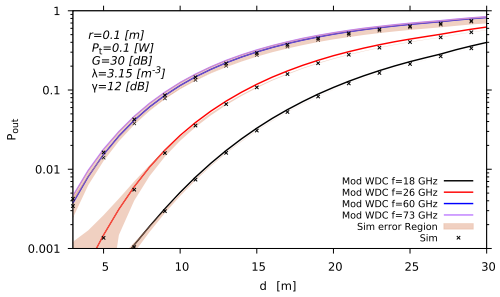

FIGURE 13. Model and simulation with 95% confidence intervals estimates of outage probability in a 3D room of 20m ×30m ×3m, for spherical obstructions, for different frequencies and their corresponding values of z, versus d_1, for best path selection.

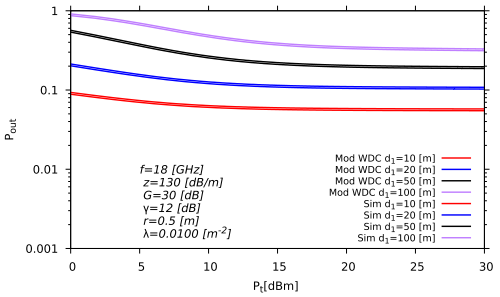

FIGURE 14. Model and simulation estimates of outage probability in a 100 m long street, for various values of link length, for circular obstructions, with best path selection, versus transmission power, for $f = 18$ GHz.

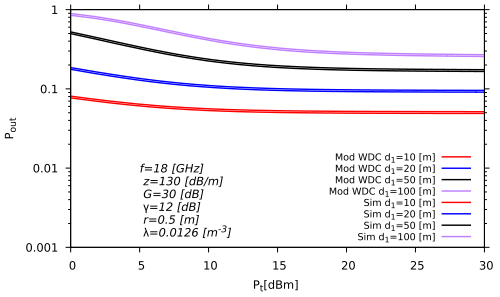

FIGURE 15. Model and simulation estimates of outage probability in a 100 m long street, for various values of link length, for spherical obstructions, with best path selection, versus transmission power, for $f = 18$ GHz.

than the one due to a sphere with the same radius. This can be intuitively explained by considering that the intersection of sphere with plane is a circle or radius equal or smaller than the radius of the sphere itself (see the Appendix for the exact expressions of the distribution in the two cases). This result raises important questions on the practical relevance of works that are based on 2D models as approximations of 3D environments. With our analytical tool it is possible to study without restrictions both 2D and 3D cases, thus allowing a correct modeling of the environment of interest.

To evaluate the impact of distance between transmitter and receiver in 3D, FIGURE 13 depicts the outage probability for different mmwave frequencies, and extends the results previously discussed for the 2D case in FIGURE 10. The figure confirms that outage probability increases fast with frequency, although there are no substantial differences between 60 and 73 GHz. With 3D obstructions and reflections, and with the parameters used in the example, the distance between transmitter and receiver that guarantees outages below 10% in the presence of randomly located obstructions is quite short (still it is much higher than in the corresponding 2D case of FIGURE 10): about 9 m with 60 or 73 GHz, 14 m at 26 GHz and as much as 20 m at 18 GHz. This means that what should drive most the selection of a mmwave frequency is the distance between transmitter and receiver, at least when coverage is the target.

C. THE 2D & 3D OUTDOOR CASES

To further showcase the potential of our approach, we consider the case of a large outdoor environment, in which we assume that only a few reflections can be used. Specifically, FIGURE 14 shows the outage probability (model and Matlab simulations) for circular obstructions in an outdoor environment consisting in a road segment with length 100 m and width 20 m, where Tx is placed at the beginning of the road, at coordinates (1, 10), and Rx is placed at a variable distance $d \in \{10, 20, 50, 100\}$ m, parallel to the horizontal axis of the road at coordinates $(1 + d, 10)$. Only reflections on the road sides are considered, and the frequency used is $f = 18$ GHz. The transmission power is varied from 1 mW to 1 W, and circular objects are large, representing, e.g. small cars, with a radius $r = 0.5$. The density of obstruction is kept low, with $\lambda = 0.0100$, which results in one obstruction within 100 meters, on average, and a probability to have no obstructions at 10 m equal to 91%.

The figure shows that the outage probability strongly depends on distance, whereas the impact of the transmission power P_t is somehow limited. In fact, increasing the transmission power decreases the outage only up to a limited extent, and only for small values of the power. In practice, this is due to the very high obstruction attenuation, which is of the order of a few hundreds of decibels per meter ($z = 130$ dB/m in the specific example), and to the fact that obstructions are big (they have meter-long diameters in the considered case). Thereby, as soon as the probability of having one or more obstructions is high, the resulting attenuation is of the order of several tens of decibels or more with high probability. Thus, to notice improvements by adjusting P_t, we would need to use several tens of dBm units of power, which means using powers in the order of kW or MW! With acceptable power levels, the outage probability cannot be driven much below the probability to have obstructions. For instance, in the 10 m case, the figure reports an outage probability as low as 6%, which is in the same order of magnitude as the probability to see at least one obstruction on the direct path, which is 9%. This is an environment where it can be reasonable to use the boolean models that appeared in the literature.

FIGURE 15 shows the outage probability (model and Matlab simulations) for spherical obstructions ($r = 0.1$ m) in an

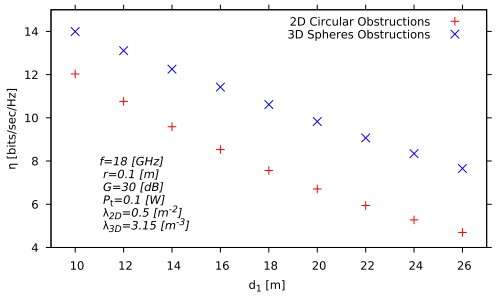

FIGURE 16. Model estimates of spectral efficiency for 2D circular obstructions and 3D spherical obstructions in the indoor cases. Results are obtained using all available reflections at $f = 18$ GHz, versus the direct distance between transmitter and receiver.

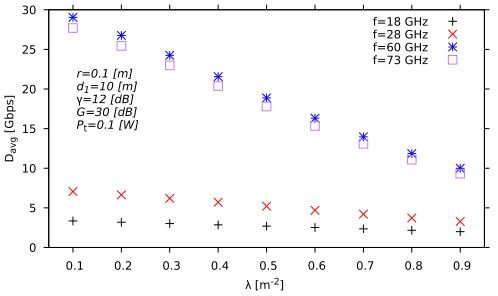

FIGURE 17. Model estimates of average rate for 2D circular obstructions in the indoor scenario, with best path selection, versus λ.

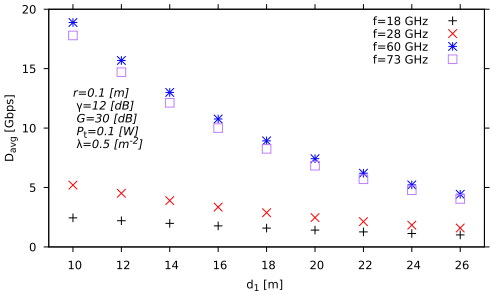

FIGURE 18. Model estimates of average rate for 2D circular obstructions in the indoor scenario, with best path selection, versus d_1.

outdoor environment of a road segment with length 100 m and width 20 m with the same power configuration used for the 2D outdoor environment discussed before. The Tx is placed at the beginning of the road at coordinates (1, 10, 2), and Rx is placed at a variable distance d (we use 10, 20, 50, 100 m), parallel to the horizontal axis of the road, at coordinates $(1+d, 10, 2)$. Similar to the 2D outdoor case, only reflections on the road sides are considered, so that the height of the volume of space considered is not important. The frequency used is $f = 18$ GHz. The results are plotted vs the transmission power, and they are similar to the ones observed for the 2D case, except the outage probability with 3D obstructions is slightly lower than with 2D obstructions. In fact, although we used the same average number of obstructions in the two cases, and the same radius, the average per-obstruction length is lower with spheres than with circles, as explained before.

D. SPECTRAL EFFICIENCY AND AVERAGE DATA RATE

To conclude our numerical evaluation, we now describe a possible application of our models. In particular, we use the outage probability result obtained with our models to calculate spectral efficiency and average rate of a mmwave link in the presence of randomly located obstructions. The key observation that we use here is that the outage probability formula can be interpreted as a function of the SNR threshold: such function is the CDF of the SNR. In fact, by denoting x as the argument of the outage probability, we have $P_{\text{out}}(x) = \Pr(\text{SNR} \leq x)$, which coincides with the definition of the CDF of the r.v. SNR computed at x.

For what concerns the spectral efficiency η, in bit/s/Hz, we can simply average the Shannon formula over possible values of SNR:

$$\eta = \int_0^\infty \log_2(1+x)\frac{dP_{\text{out}}(x)}{dx}dx. \tag{31}$$

As an example, FIGURE 16 provides model estimates for the spectral efficiency in the presence of 2D circular obstructions or 3D spherical obstructions at $f = 18$ GHz (for $z = 130$ dB/m), at various values of the distance between transmitter and receiver. The reference scenarios are the ones considered for indoor cases earlier in this section, with $\gamma_{\text{th}} = 12$. The figure shows a monotonic decrease of spectral efficiency with distance.

The spectral efficiency for 3D spherical obstructions is higher than the one with 2D circular obstructions, for the same reasons already mentioned in the discussion of the results in FIGURE 11. This further proves that selecting the least attenuated path with beamsteering offers a significant diversity gain.

Eventually, we consider the average data rate D_{avg} that can be achieved with spectral efficiency η and with the modulated bandwidth that can be offered at the different mmwave carriers:

$$D_{\text{avg}} = \eta \cdot W, \tag{32}$$

where W is the available bandwidth, for which we consider 200 MHz, 500 MHz, 2.6 GHz, and 2.6 GHz at, respectively, 18, 28, 60 and 73 GHz [31].

FIGURE 17 illustrates the case with 2D circular obstructions, as a function of λ. Here the fact that higher mmwave frequencies allow for wider bandwidth modulated signals turns into higher data rates, irrespective of obstruction density. So, in terms of data rate, at a given distance and SNR threshold, the higher the frequency the better.

If we change the distance d, we obtain the results plotted in FIGURE 18. Also here, for fixed values of λ and γ_{th}, higher frequencies are more convenient at all distances. These results on spectral efficiency and data rate tell that higher frequencies

should be used as much as possible also in the presence of randomly located obstructions. Interestingly, all results discussed in this subsection, obtained as in a corollary from our outage probability models, show that higher mmwave frequencies always offer higher performance figures also in the presence of obstructions, at least in practical scenarios as the ones tackled in this work.

VI. CONCLUSION

In this article we have proposed a methodology to stochastically model the impact of attenuation in mmwave links due to randomly located obstructions. Differently from existing models, we do not consider the presence of an obstruction as a binary variable that causes outage, but we rather account for the cumulative attenuation caused by multiple objects, depending on the obstruction lengths that we characterize stochastically. We have proposed two modeling approaches to reduce the complexity of calculating the distribution of outage. A simple approximation is based on considering the distribution of the number of objects on a path, each obstructing proportionally to its average chord length. A more complex, yet tractable approach is based on the use of weighted Dirac combs to approximate the chord length distribution, which generalizes the simple approach. The resulting models are oblivious to the shape of obstructions, and indeed we have provided general expressions for all shapes, and specific refined expressions for convex shapes. The models apply to both 2D and 3D descriptions of the mmwave environment and of obstructions.

We have numerically evaluated the accuracy of the models and the performance of mmwave links in a large set of realistic scenarios. We have proven the usefulness of our model by comparing analytical predictions against simulation results, and the advantages offered by the weighted Dirac comb-based approximation.

With the models, we have explored the impact of distance, obstruction shape, size and density, and mmwave frequencies and modulated bandwidths. Our results show the extremely high convenience of beamsteering antennas along direct and primary reflection directions, based on the fading-average path attenuation, which can easily be done in current off-the-shelf mmwave devices. We have also shown that lower frequencies are convenient when it comes to offer coverage, i.e., to extend the range of mmwave links when no data rate needs to be guaranteed, although higher frequencies are always convenient in terms of average achieved data rate.

ACKNOWLEDGMENT

This article was presented in part at ACM mmNets'19.

APPENDIX A CHORD LENGTH DISTRIBUTIONS

The chord length distribution (which is the obstruction length distribution in our case) is known for some regular 2D and 3D shapes.

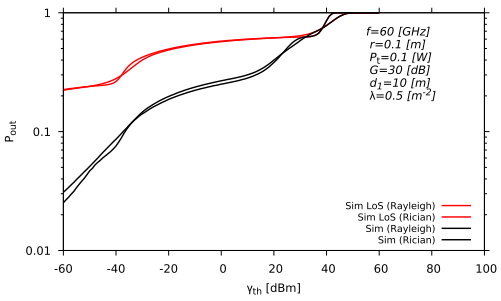

FIGURE 19. Simulation of outage probability for circular obstructions having LoS with rayleigh and rice fading.

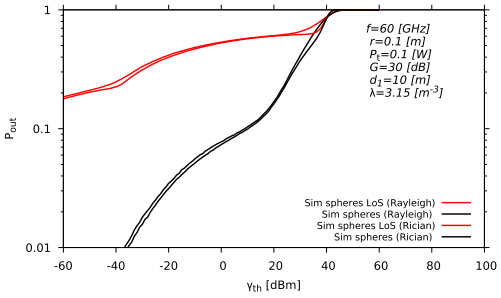

FIGURE 20. Simulation of outage probability for spherical obstructions having LoS with rayleigh and rice fading.

For circular obstructions of radius r, the distribution is given by [32]:

$$f_\ell(x) = \frac{x}{2r\sqrt{4r^2-x^2}}, \quad 0 < x \leq 2r. \tag{33}$$

For square obstructions of side length l, we have [32]:

$$f_\ell(x) = \begin{cases} \frac{1}{2l}, & 0 < x \leq l; \\ \frac{l^2}{x^2\sqrt{x^2-l^2}} - \frac{1}{2l}, & l < x \leq \sqrt{2}l. \end{cases} \tag{34}$$

For what concerns spheres, as mentioned in [11], the chord length distribution depends on the definition of the process that generates the random lines that form the chord by intersecting the sphere. We consider the case in which straight lines are uniformly distributed in $\mathbb{R}^3$. Thus, the obstruction length distribution is expressed as follows:

$$f_\ell(x) = \frac{x}{2r^2}, \quad 0 < x \leq 2r. \tag{35}$$

For cubes of side l, the obstruction length distribution has the following form, which has been taken from [33] (36), as shown at the top of the next page.

APPENDIX B RAYLEIGH vs RICE LOS FADING

In our models, for tractability reasons, we have used Rayleigh fading in all cases. However, it is well known that LoS links experience Rice fading when components from reflections are much lower then the LoS component. Here we use simulations to show that our approximation does not impact the quality of the results derived in this work. Specifically, FIGURES 19 and 20 report simulation results obtained with Rayleigh and Rice fading for the LoS path, for 2D and 3D

$$f_\ell(x)=\begin{cases}\dfrac{8\left(\frac{x}{l}\right)^3-3\left(\frac{x}{l}\right)^4}{3\pi\left(\frac{x}{l}\right)^3}, & \text{for } 0<x\le l;\\ \dfrac{6\pi+6\left(\frac{x}{l}\right)^4-1-8\left[2\left(\frac{x}{l}\right)^2+1\right]\sqrt{\left(\frac{x}{l}\right)^2-1}}{3\pi\left(\frac{x}{l}\right)^3}, & \text{for } l<x\le\sqrt{2}l;\\ \dfrac{6\pi-3\left(\frac{x}{l}\right)^4-5+8\left[\left(\frac{x}{l}\right)^2+1\right]\sqrt{\left(\frac{x}{l}\right)^2-2}-24\arctan\left(\sqrt{\left(\frac{x}{l}\right)^2-2}\right)}{3\pi\left(\frac{x}{l}\right)^3} & \text{for } \sqrt{2}l<x\le\sqrt{3}l.\end{cases} \tag{36}$$

configurations, respectively, and for both the cases when considering the LoS link only, and when using beamforming over the least attenuated path. As can observed in the figures, simulations show minor differences. This behaviour is due to the fact that the main contribution to outage is due to obstructions, while fading has a lesser role.

REFERENCES

[1] A. A. AbdelNabi, V. Mancuso, and M. A. Marsan, "On the outage probability of millimeter wave links with quasi-deterministic propagation," in *Proc. 3rd ACM Workshop Millim.-wave Netw. Sens. Syst. (mmNets)*. New York, NY, USA: Association for Computing Machinery, 2019, pp. 1–6, doi: 10.1145/3349624.3356762.

[2] (Feb. 2020). *Cisco Annual Internet Report (2018–2023) White Paper*. [Online]. Available: https://www.cisco.com/c/en/us/solutions/collateral/executive-perspectives/annual-internet-report/white-paper-c11-741490.html

[3] P. Cerwall. (Nov. 2019). *Ericsson Mobility Report*. [Online]. Available: https://www.ericsson.com/491b06/assets/local/mobility-report/documents/2019/ericsson-mobility-report-q4-2019-update.pdf

[4] M. Bennis, M. Debbah, and H. V. Poor, "Ultrareliable and low-latency wireless communication: Tail, risk, and scale," *Proc. IEEE*, vol. 106, no. 10, pp. 1834–1853, Oct. 2018.

[5] T. S. Rappaport, S. Sun, R. Mayzus, H. Zhao, Y. Azar, K. Wang, G. N. Wong, J. K. Schulz, M. Samimi, and F. Gutierrez, "Millimeter wave mobile communications for 5G cellular: It will work!," *IEEE Access*, vol. 1, pp. 335–349, 2013.

[6] J. G. Andrews, T. Bai, M. N. Kulkarni, A. Alkhateeb, A. K. Gupta, and R. W. Heath, Jr., "Modeling and analyzing millimeter wave cellular systems," *IEEE Trans. Commun.*, vol. 65, no. 1, pp. 403–430, Jan. 2017.

[7] M. Agiwal, A. Roy, and N. Saxena, "Next generation 5G wireless networks: A comprehensive survey," *IEEE Commun. Surveys Tuts.*, vol. 18, no. 3, pp. 1617–1655, 3rd Quart., 2016.

[8] T. S. Rappaport and S. Deng, "73 GHz wideband millimeter-wave foliage and ground reflection measurements and models," in *Proc. IEEE Int. Conf. Commun. Workshop (ICCW)*, Jun. 2015, pp. 1238–1243.

[9] R. J. Weiler, M. Peter, W. Keusgen, A. Maltsev, I. Karls, A. Pudeyev, I. Bolotin, I. Siaud, and A.-M. Ulmer-Moll, "Quasi-deterministic millimeter-wave channel models in MiWEBA," *EURASIP J. Wireless Commun. Netw.*, vol. 2016, no. 1, p. 84, Mar. 2016.

[10] T. Bai and R. W. Heath, Jr., "Analysis of self-body blocking effects in millimeter wave cellular networks," in *Proc. 48th Asilomar Conf. Signals, Syst. Comput.*, Nov. 2014, pp. 1921–1925.

[11] K. Rizk, J.-F. Wagen, and F. Gardiol, "Two-dimensional ray-tracing modeling for propagation prediction in microcellular environments," *IEEE Trans. Veh. Technol.*, vol. 46, no. 2, pp. 508–518, May 1997.

[12] K. Han, K. Huang, and R. W. Heath, Jr., "Connectivity and blockage effects in millimeter-wave air-to-everything networks," *IEEE Wireless Commun. Lett.*, vol. 8, no. 2, pp. 388–391, Apr. 2019.

[13] T. Bai, R. Vaze, and R. W. Heath, Jr., "Analysis of blockage effects on urban cellular networks," *IEEE Trans. Wireless Commun.*, vol. 13, no. 9, pp. 5070–5083, Sep. 2014.

[14] K. Venugopal and R. W. Heath, "Millimeter wave networked wearables in dense indoor environments," *IEEE Access*, vol. 4, pp. 1205–1221, 2016.

[15] J. Ryan, G. R. MacCartney, and T. S. Rappaport, "Indoor office wideband penetration loss measurements at 73 GHz," in *Proc. IEEE Int. Conf. Commun. Workshops (ICC Workshops)*, May 2017, pp. 228–233.

[16] G. R. MacCartney, S. Deng, S. Sun, and T. S. Rappaport, "Millimeter-wave human blockage at 73 GHz with a simple double knife-edge diffraction model and extension for directional antennas," in *Proc. IEEE 84th Veh. Technol. Conf. (VTC-Fall)*, Sep. 2016, pp. 1–6.

[17] V. Raghavan, L. Akhoondzadeh-Asl, V. Podshivalov, J. Hulten, M. A. Tassoudji, O. H. Koymen, A. Sampath, and J. Li, "Statistical blockage modeling and robustness of beamforming in millimeter-wave systems," *IEEE Trans. Microw. Theory Techn.*, vol. 67, no. 7, pp. 3010–3024, Jul. 2019.

[18] I. Kumar Jain, R. Kumar, and S. Panwar, "Limited by capacity or blockage? A millimeter wave blockage analysis," 2018, *arXiv:1808.01228*. [Online]. Available: http://arxiv.org/abs/1808.01228

[19] M. K. Muller, S. Schwarz, and M. Rupp, "Investigation of area spectral efficiency in indoor wireless communications by blockage models," in *Proc. 16th Int. Symp. Model. Optim. Mobile, Ad Hoc, Wireless Netw. (WiOpt)*, May 2018, pp. 1–6.

[20] B. Peng, S. Rey, D. M. Rose, S. Hahn, and T. Kuerner, "Statistical characteristics study of human blockage effect in future indoor millimeter and sub-millimeter wave wireless communications," in *Proc. IEEE 87th Veh. Technol. Conf. (VTC Spring)*, Jun. 2018, pp. 1–5.

[21] M. Zarifneshat, P. Roy, and L. Xiao, "Multi-objective approach to improve load balance and blockage in millimeter wave cellular networks," in *Proc. IEEE Int. Symp. Dyn. Spectr. Access Netw. (DySPAN)*, Nov. 2019, pp. 1–10.

[22] M. Dong and T. Kim, "Reliability of an urban millimeter wave communication link with first-order reflections," in *Proc. IEEE Global Commun. Conf. (GLOBECOM)*, Dec. 2016, pp. 1–6.

[23] T. Nitsche, C. Cordeiro, A. Flores, E. Knightly, E. Perahia, and J. Widmer, "IEEE 802.11ad: Directional 60 GHz communication for multi-gigabit-per-second Wi-Fi [invited paper]," *IEEE Commun. Mag.*, vol. 52, no. 12, pp. 132–141, Dec. 2014.

[24] C. A. Balanis, *Antenna Theory: Analysis and Design*. Hoboken, NJ, USA: Wiley, 2016.

[25] V. Petrov, M. Komarov, D. Moltchanov, J. M. Jornet, and Y. Koucheryavy, "Interference and SINR in millimeter wave and terahertz communication systems with blocking and directional antennas," *IEEE Trans. Wireless Commun.*, vol. 16, no. 3, pp. 1791–1808, Mar. 2017.

[26] D. A. Klain and G.-C. Rota, *Introduction to Geometric Probability*. Cambridge, U.K.: Cambridge Univ. Press, 1997.

[27] S. Sun, H. Yan, G. R. MacCartney, and T. S. Rappaport, "Millimeter wave small-scale spatial statistics in an urban microcell scenario," in *Proc. IEEE Int. Conf. Commun. (ICC)*, May 2017, pp. 1–7.

[28] D. G. Rees, *Essential Statistics*. New York, NY, USA: Springer, 1989.

[29] S. J. Dudzinsky, "Atmospheric effects on terrestrial millimeter-wave communications," in *Proc. 4th Eur. Microw. Conf.*, Oct. 1974, pp. 197–201.

[30] *IEEE Standard for Information Technology–Telecommunications and Information Exchange Between Systems–Local and Metropolitan Area Networks–Specific Requirements-Part 11: Wireless LAN Medium Access Control (MAC) and Physical Layer (PHY) Specifications Amendment 3: Enhancements for Very High Throughput in the 60 GHz Band*, IEEE Standard 802.11ad-2012, Dec. 2012.

[31] "Fixed service use and future trends," Int. Telecommun. Union Radiocommun. Sector, F-series, ITU, Geneva, Switzerland, Tech. Rep. ITU-R F.2323-0, 2014.

[32] D. Stoyan and H. Stoyan, *Fractals, Random Shapes and Point Fields: Methods of Geometrical Statistics* (Wiley Series in Probability and Mathematical Statistics: Applied Probability and Statistics). Hoboken, NJ, USA: Wiley, 1994.

[33] D. W. Jokisch, P. W. Patton, D. A. Rajon, B. A. Inglis, and W. E. Bolch, "Chord distributions across 3D digital images of a human thoracic vertebra," *Med. Phys.*, vol. 28, no. 7, pp. 1493–1504, Jul. 2001.

AMR A. ABDELNABI received the M.Sc. degree in electrical engineering from Nile University, Cairo, Egypt, in 2012. He is currently pursuing the Ph.D. degree with UC3M, Spain. He has served as a Radio Planning Engineer for WCDMA Networks with Vodafone, Egypt, and as a Radio Optimization Expert for WCDMA networks in Mobinil, an Orange subsidiary in Egypt. From October 2013 to September 2015, he worked as a Research Associate with Texas A&M University, Qatar. He is also a Research Assistant with the IMDEA Networks Institute. His research interests include stochastic geometry and its application to wireless networks, channel modeling, interference modeling, MIMO communication systems, cooperative communications, device-to-device communication, applied signal processing, compressed sensing, and machine learning.

VINCENZO MANCUSO (Member, IEEE) received the M.Sc. and Ph.D. degrees in electronics, computer science and telecommunications from the University of Palermo, Italy. He is currently a Research Associate Professor with the IMDEA Networks Institute, Spain. Previously, he was with INRIA Sophia Antipolis, France, Rice University, Houston, TX, USA, and the University of Palermo. He has authored more than 110 peer-reviewed publications focusing on Internet QoS and on the analysis, design, and experimental evaluation of opportunistic and adaptive protocols and architectures for wireless networks. He is also working on analysis and optimization of wireless access networks and on the measurements and assessment of mobile broadband networks. He was a recipient of a Ramon y Cajal Research Grant of the Spanish Ministry of Science and Innovation.

MARCO AJMONE MARSAN (Life Fellow, IEEE) received the honorary degree in telecommunication networks from the Budapest University of Technology and Economics. He has been with the Politecnico di Torino, Italy, since 1974, with an interruption, from 1987 to 1990, when he was a Full Professor with the Computer Science Department, University of Milan. He is currently a Full Professor with the Politecnico di Torino, and a part-time Research Professor with the IMDEA Networks Institute, Leganés, Spain. He has published over 400 articles in the leading conferences and journals of his research area as well as two books. He is a member of the Academia Europaea and the Academy of Sciences of Torino. He has been the Chair of the steering committee of the ACM/IEEE TRANSACTIONS ON NETWORKING. He is a member of the editorial boards of *Computer Networks* and *Performance Evaluation* of Elsevier and ACM TOMPECS. He was the General Chair of INFOCOM 2013.